Supplementary Information for:

Aircraft measurements of aerosol and trace gas chemistry in the Eastern North Atlantic

Maria A. Zawadowicz[1], Kaitlyn Suski[1,c], Jiumeng Liu[1,b], Mikhail Pekour[1], Jerome Fast[1], Fan Mei[1], Arthur Sedlacek[2], Stephen Springston[2], Yang Wang[3,a], Rahul A. Zaveri[1], Robert Wood[4], Jian Wang[3], John E. Shilling[1]

[1]Atmospheric Sciences and Global Change Division, Pacific Northwest National Laboratory, Richland, WA, 99352, USA
[2]Environmental & Climate Sciences Department, Brookhaven National Laboratory, Upton, NY 11973, USA
[3]Department of Energy, Environmental and Chemical Engineering, Washington University in St. Louis, Saint Louis, MO, 63130, USA
[4]Department of Atmospheric Science, University of Washington, Seattle, WA, 98195, USA

[a]Now at: Department of Civil, Architectural and Environmental Engineering, Missouri University of Science and Technology, Rolla, MO, 65409, USA
[b]Now at: School of Environment, Harbin Institute of Technology, Harbin, Heilongjiang, China.
[c]Now at: JUUL Labs, San Francisco, CA, 94107, USA

Correspondence to: John E. Shilling (john.shilling@pnnl.gov)

AMS calibration for quantification of methanesulfonic acid (MSA)

There are several published methods of calibrating the AMS signal for the presence of MSA (Phinney et al., 2006, Huang et al., 2017, Ovadnevaite et al., 2011, Ge et al., 2012, Hodshire et al., 2019), but they all concentrate on the presence of a characteristic MSA marker, $CH_3SO_2^+$. In addition, there are two additional minor characteristic markers, $CH_2SO_2^+$ and $CH_4SO_3^+$ (Ge et al., 2012, Huang et al., 2017). A well-known difficulty in laboratory MSA calibrations is neutralization of the acidic aerosol by the presence of trace amount of ammonia in laboratory air and on surfaces (Hodshire et al., 2019). To overcome this difficulty, we adapt the approach detailed in Hodshire, et al. (2019) and first calibrate the AMS using the neutralized form of MSA, $NH_4CH_3SO_3$. To prepare the calibration solution, MSA was neutralized with ammonium hydroxide. The final concentration of the calibration solution was 75 mM. The calibration solution was aerosolized with a Collison-type atomizer (TSI 3076, Shoreview, MN) and dried using a Nafion dryer (5 slpm counter-flow). The resulting aerosol was size-selected with a Differential Mobility Analyzer (DMA) (TSI, Shoreview, MN) to 250, 300 and 350 nm (Supplementary Figure S2). The calibration was performed using simultaneous measurements of $CH_3SO_3^-$ ion concentration derived from Condensation Particle Counter (CPC) particle counts (TSI 3776, Shoreview, MN). In order to derive $CH_3SO_3^-$ ion concentration, density of 1.3 g/cm^3 and shape factor of 1 was assumed. AMS PTOF data were used to correct for multiply charged particles. Resulting calibrations are shown in Supplementary Figure S2, along with a reference AMS mass spectrum of laboratory-generated neutralized MSA.

To quantify MSA, we use the combination of the three characteristic marker ions ($CH_2SO_2^+$ + $CH_3SO_2^+$ + $CH_4SO_3^+$). Using the standard AMS approach, (neutralized) MSA concentration is given by

$$[MSA] = \frac{C}{CE}\frac{MW_{NO_3}}{RIE_{MSA}IE_{NO_3}}\frac{I_{CH_2SO_2}+I_{CH_3SO_2}+I_{CH_4SO_3}}{f_{(CH_2SO_2+CH_3SO_2+CH_4SO_3)}},$$

Where C is a proportionality constant accounting for instrument duty cycle, flow rate and unit conversions. CE is the AMS collection efficiency, RIE_{MSA} is the ionization efficiency of (neutralized) MSA expressed proportionally to the ionization efficiency of nitrate (IE_{NO_3}), which is obtained by standard AMS NH_4NO_3 calibration. I_x expresses the signal of marker ion x in ion counts and $f_{(CH_2SO_2+ CH_3SO_2+CH_4SO_3)}$ is the ratio of signal of the sum of the marker ions to the total (neutralized) MSA signal. If ion signal is expressed in nitrate-equivalent concentration units, the equation simplifies to

$$[MSA] = \frac{1}{CE\ RIE_{MSA}\ f_{(CH_2SO_2+CH_3SO_2+CH_4SO_3)}}\left(I_{CH_2SO_2}+I_{CH_3SO_2}+I_{CH_4SO_3}\right) = \frac{CF}{CE}\left(I_{CH_2SO_2}+I_{CH_3SO_2}+I_{CH_4SO_3}\right)$$

Where $CF = \frac{1}{RIE_{MSA}\ f_{(CH_2SO_2+CH_3SO_2+CH_4SO_3)}}$ is defined as the calibration factor and $\frac{CF}{CE}$ the slope in the laboratory calibration plot in Supplementary Figure S2, and has been determined to be 7.2 ± 0.9.

Next, we determine parameters RIE_{MSA}, $f_{(CH_2SO_2+ CH_3SO_2+CH_4SO_3)}$ and $f_{CH_3SO_2}$ directly and summarize then in Supplementary Table S2. The ratios of marker signals to the total (neutralized) MSA signal are derived from average neutralized MSA mass spectra (Supplementary Figure S2A). RIE_{MSA} can be estimated with the ammonium balance method: using the previously calibrated RIE_{NH_4} (4.1), RIE_{MSA} is adjusted to balance the ammonium with its counter-ion, $CH_3SO_3^-$. This assumes complete neutralization of MSA in the AMS. Supplementary Table S2 compares these calibration parameters to previous literature estimates, showing a large spread in values, which underscores the importance of calibrating each AMS independently.

Using the slope of the calibration plot in Figure S2B and independently derived estimates of RIE_{MSA} and $f_{(CH_2SO_2+ CH_3SO_2+CH_4SO_3)}$, we can constrain the CE for the neutralized MSA used in laboratory calibrations as 0.61 ± 0.07. This is the largest source of uncertainty in translating the calibrations to ambient measurements of MSA, as ambient MSA is more acidic than the neutralized laboratory MSA, which is expected to affect CE (Middlebrook et al., 2012). If the CE of acidic form of MSA is assumed to be 1, the calibration factor CF is 4.4 ± 0.5, as shown in Figure S2C. This CE-corrected calibration factor is used to translate ACE-ENA AMS measurements to MSA concentrations.

Using the laboratory MSA calibrations, we also calculate the fraction of MSA signal assigned to organic and sulfate, 64% and 36%, respectively (Supplementary Table S2). Some MSA ions, such as the three characteristic markers used in the calibration are organosulfates, which are classified as organic by the default AMS routine.

Supplementary Table S1: Summary of ACE-ENA flights and vertical profiles.

RF #	Flight date	Takeoff (local time)	Landing (local time)	Number of spiral profiles	Location of spiral profiles (lat, lon)
summer					
1	6/21/17	11:28	15:10	2	39.2273, -28.351
					39.2436, -28.3691
2	6/23/17	10:46	14:04	4	39.105, -28.0321
					39.7931, -29.534
					39.1137, -28.018
					39.1796, -28.1548
3	6/25/17	10:34	14:25	2	39.1142, -28.0365
					39.7511, -29.2662
4	6/26/17	8:30	12:15	2	39.1567, -28.185
					39.2634, -28.3962
5	6/28/17	9:07	12:29	2	39.2738, -28.306
					39.3055, -27.7953
6	6/29/17	10:30	14:34	2	40.09, -28.0557
					40.1092, -28.0242
7	6/30/17	9:27	13:16	2	39.2975, -27.7847
					39.3034, -28.3341
8	7/3/17	10:37	14:48	2	39.105, -28.0098
					39.1018, -28.0254
9	7/4/17	8:33	12:06	4	39.3201, -28.3033
					38.9714, -28.2459
					39.3126, -28.3023
					38.9436, -28.2443
10	7/6/17	8:23	11:48	3	39.3458, -28.0354
					39.365, -28.0098
					39.3672, -28.0189
11	7/7/17	10:33	13:49	2	37.7564, -27.143
					37.5056, -26.8463
12	7/8/17	8:36	12:43	4	40.0172, -27.1451
					39.5961, -26.6761
					39.4637, -26.5093
					39.8162, -25.7871

13	7/11/17	10:04	14:04	2	39.3241, -28.2765
					39.3404, -28.2629
14	7/12/17	9:00	13:02	2	39.253, -28.0551
					39.2658, -28.0466
15	7/13/17	8:32	12:55	3	39.3268, -27.8833
					39.3303, -27.8537
					39.0175, -27.7892
16	7/15/17	10:24	14:24	3	39.2052, -27.8981
					39.4566, -27.9692
					39.4099, -28.0093
17	7/17/17	9:29	13:28	3	39.2072, -28.3731
					39.387, -26.6409
					39.1973, -25.8684
18	7/18/17	8:31	12:05	3	39.3412, -28.0793
					39.3042, -27.7573
					39.3083, -28.284
19	7/19/17	8:54	12:56	5	39.1734, -28.4033
					39.3882, -27.8967
					39.3846, -27.9203
					39.4504, -27.5893
					39.7882, -26.6081
20	7/20/17	8:31	12:11	3	39.2515, -27.7209
					39.2562, -27.7033
					39.3535, -28.2465
winter					
21	1/19/18	11:11	15:04	3	39.0709, -28.3686
					39.069, -28.4012
					39.0695, -28.4246
22	1/21/18	8:45	12:29	3	38.8088, -25.7359
					38.8245, -25.7392
					38.8233, -25.7022
23	1/24/18	11:53	15:54	3	39.3135, -28.2306
					39.3007, -28.2188
					39.3444, -28.1837
24	1/25/17	10:01	13:49	4	39.307, -27.8591

					39.2327, -28.3454
					39.3481, -27.8774
					39.3455, -27.8824
25	1/26/18	10:05	14:03	2	38.009, -27.1372
					37.7275, -27.9024
26	1/28/18	8:38	12:33	2	38.0474, -27.1695
					38.3184, -27.4664
27	1/29/18	8:39	12:32	3	38.9701, -27.6632
					38.9799, -27.6745
					39.3521, -27.9111
28	1/30/18	8:34	12:50	3	39.2794, -27.6507
					39.4435, -28.2626
					39.2809, -27.636
29	2/1/18	9:59	14:18	4	39.2823, -27.7286
					39.3117, -28.2559
					39.3414, -28.2303
					39.369, -27.744
30	2/7/18	16:28	18:22	0	N/A
31	2/8/18	11:54	16:04	3	39.3928, -27.9622
					39.3823, -27.9122
					39.3575, -27.9554
32	2/9/18	10:04	14:16	4	39.3611, -27.8233
					39.2537, -28.3428
					39.352, -27.7877
					39.3174, -27.8658
33	2/10/18	11:55	15:55	5	39.3423, -27.7868
					39.3063, -27.7254
					39.3128, -27.7081
					39.2434, -28.3459
					39.2174, -27.6556
34	2/11/18	10:20	14:20	5	39.1324, -28.0476
					39.1033, -28.021
					39.1121, -28.0273
					39.4414, -28.6022
					39.12, -28.0448

35	2/12/18	10:05	14:07	3	39.0698, -28.4165
					39.06, -28.4072
					39.0586, -28.3847
36	2/15/18	11:59	16:14	3	39.1701, -27.9797
					39.6477, -27.9835
					39.0632, -28.0428
37	2/16/18	11:54	16:04	4	39.3114, -27.8122
					39.2786, -27.7357
					39.1124, -28.0979
					39.2961, -27.8063
38	2/18/18	11:29	15:41	3	39.4839, -27.3574
					39.192, -28.0234
					39.4708, -28.1345
39	2/19/18	10:01	14:09	3	39.3196, -27.7709
					39.313, -27.7204
					39.3452, -27.7481

Supplementary Table S2: Calibration parameters for MSA in the PNNL AMS and comparisons to literature.

Parameter	This work	Previous estimates if available
MSA_{Org} (%)	63.9 ± 0.7	
MSA_{SO_4} (%)	36.1 ± 0.7	
RIE_{MSA} (UMR)	1.09 ± 0.02	1.33 (Willis et al., 2016), 1.27 (Huang et al., 2017), 1.70 ± 0.08 (Hodshire et al., 2019)
RIE_{MSA} (HR)	0.87 ± 0.01	
$f_{CH_3SO_2}$ (%)	15.9 ± 0.3	6.9 (Phinney et al., 2006), 9 (Zorn et al., 2008), 4 (Schmale et al., 2013), 9.7 (Huang et al., 2015), 12.4 (Willis et al., 2016), 4 (Huang et al., 2017), 7.9 (Hodshire et al., 2019)
$f_{(CH_2SO_2+CH_3SO_2+CH_4SO_3)}$ (%)	26.1 ± 0.5	14.7 (Ge et al., 2012), 6.8 ± 0.6 (Huang et al., 2017)
Calibration factor (C_F)	4.4 ± 0.5	

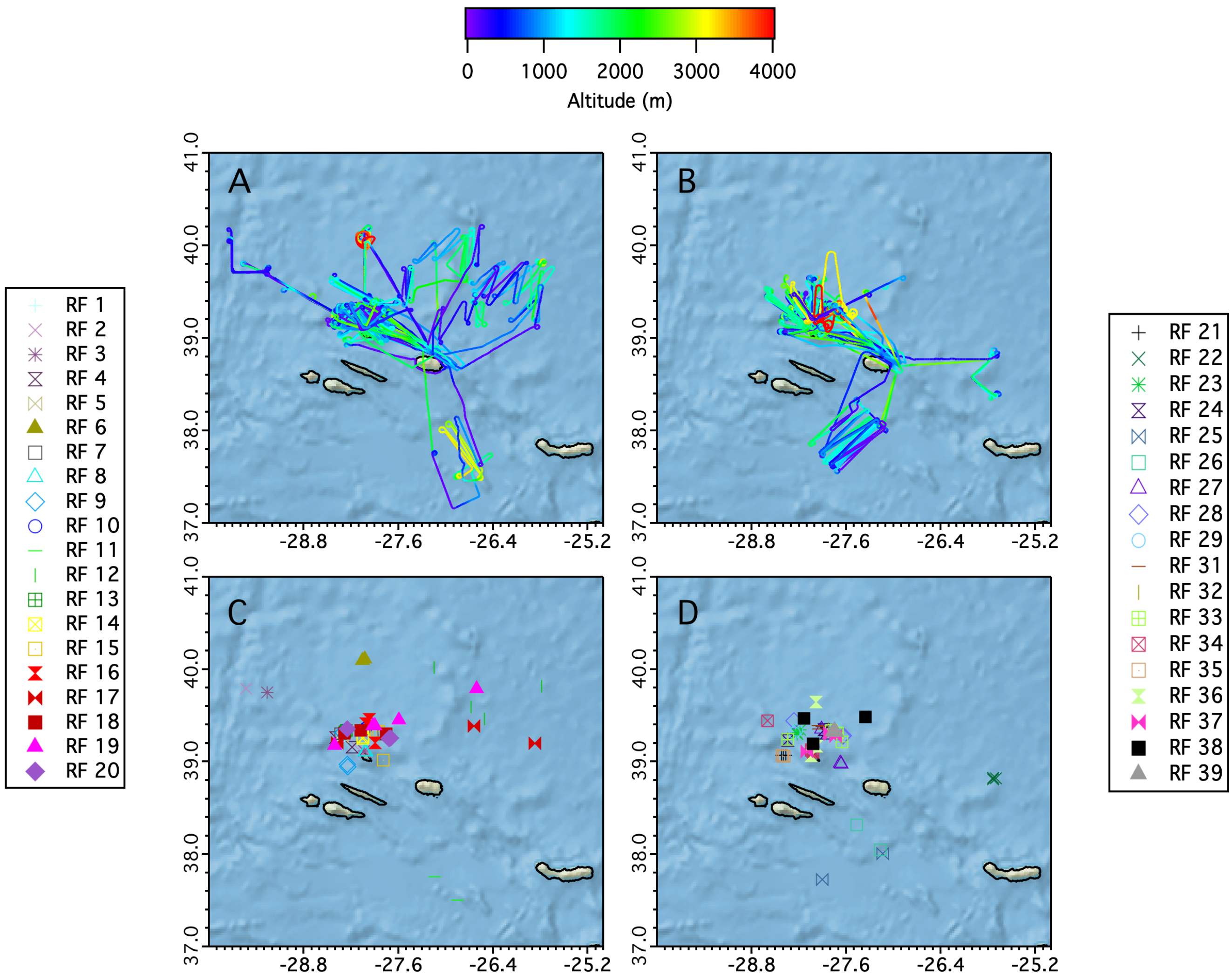

Supplementary Figure S1: Flight tracks for all G-1 flights carried out as a part of the ACE-ENA campaign. (A) All IOP 1 flight tracks. (B) All IOP 2 flight tracks. (C) Locations of spiral profiles for IOP 1. (D) Locations of spiral profiles for IOP 2. The map was created using public domain map data on Natural Earth (naturalearthdata.com) and the GSHHG Database (ngdc.noaa.gov/mgg/shorelines/).

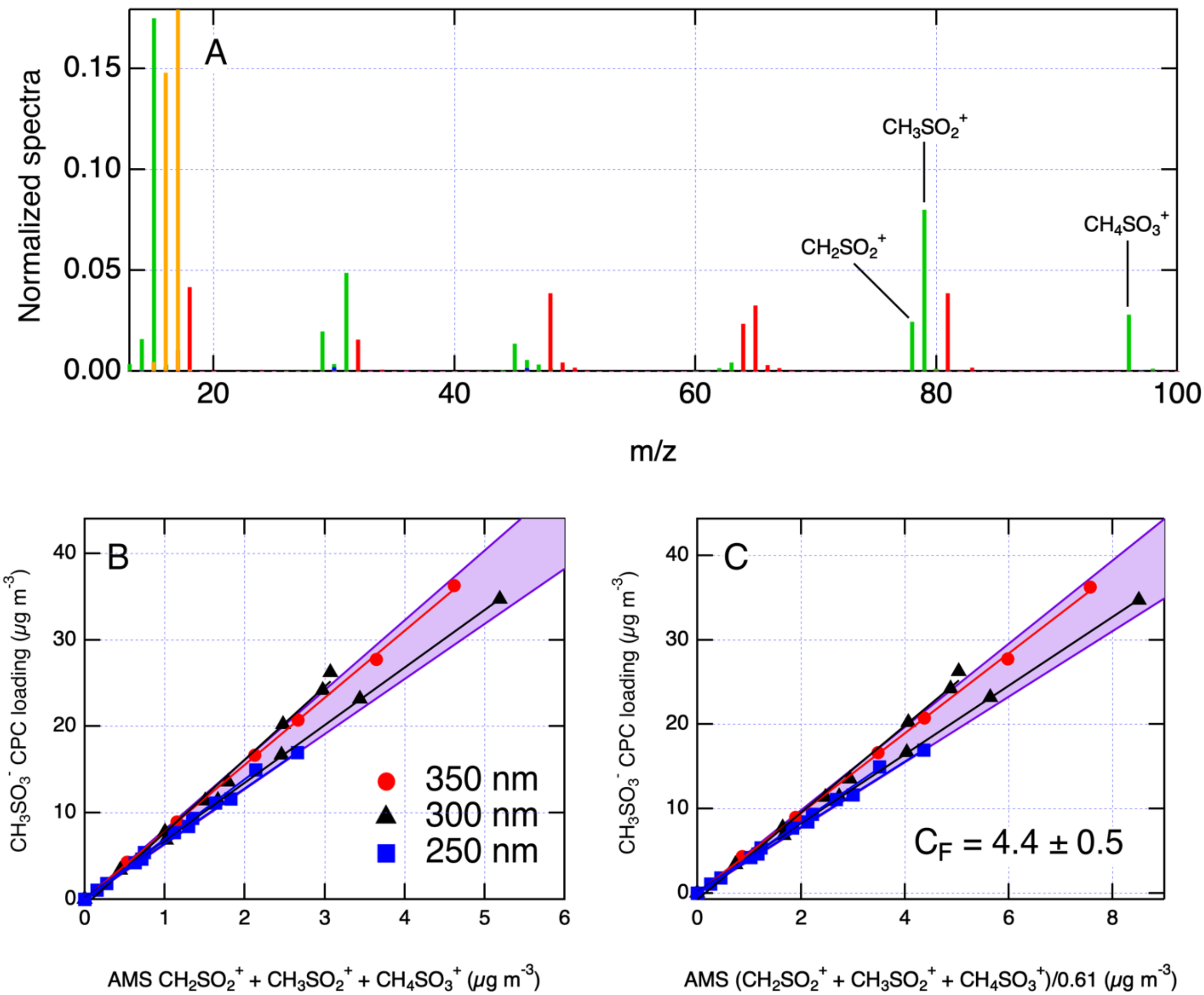

Supplementary Figure S2: Laboratory AMS calibrations for MSA. (A) Example spectrum of neutralized MSA used for the calibrations with key peaks labeled. (B) Calibrations using three different neutralized MSA sizes. Shaded region indicates uncertainty.

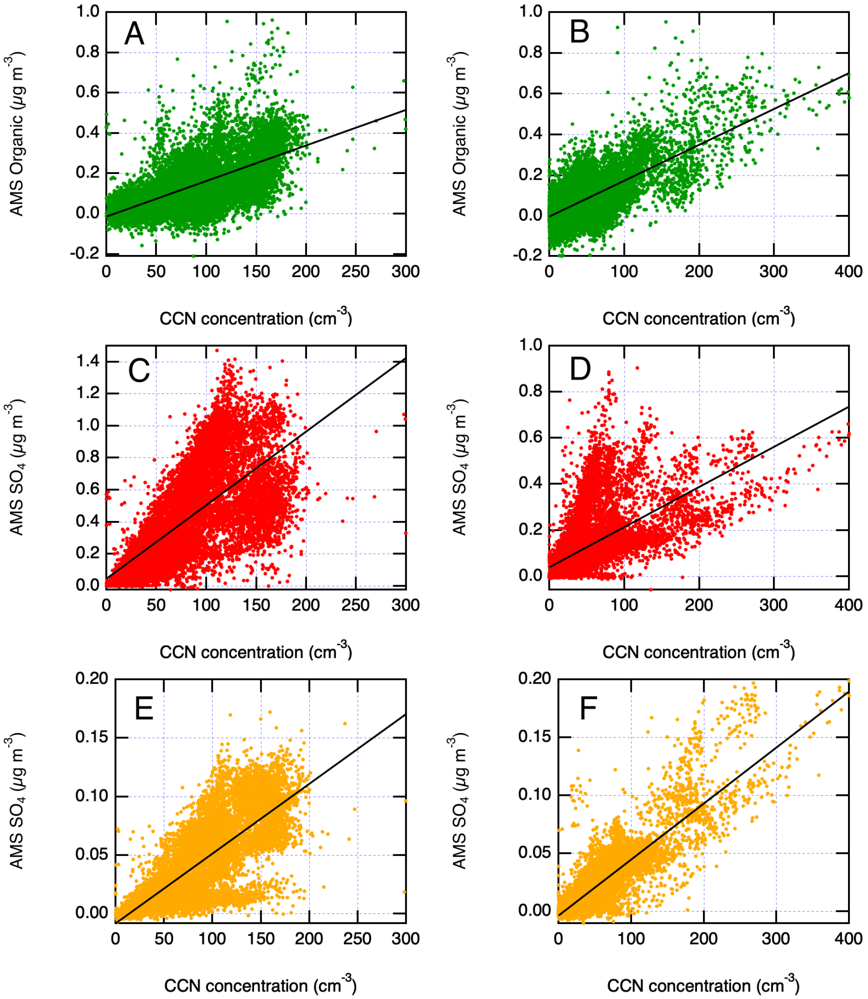

Supplementary Figure S3: Campaign-wide correlations between aerosol chemistry and CCN concentrations at 0.1% supersaturation. (A) AMS organic vs. CCN count, < 1000 m (R^2 = 0.4). (B) AMS organic vs. CCN count, > 1000 m (R^2 = 0.5). (C) AMS SO_4 vs. CCN count, < 1000 m (R^2 = 0.5). (D) AMS SO_4 vs. CCN count, > 1000 m (R^2 = 0.4). (E) AMS NH_4 vs. CCN count, < 1000 m (R^2 = 0.6). (F) AMS NH_4 vs. CCN count, > 1000 m (R^2 = 0.8).

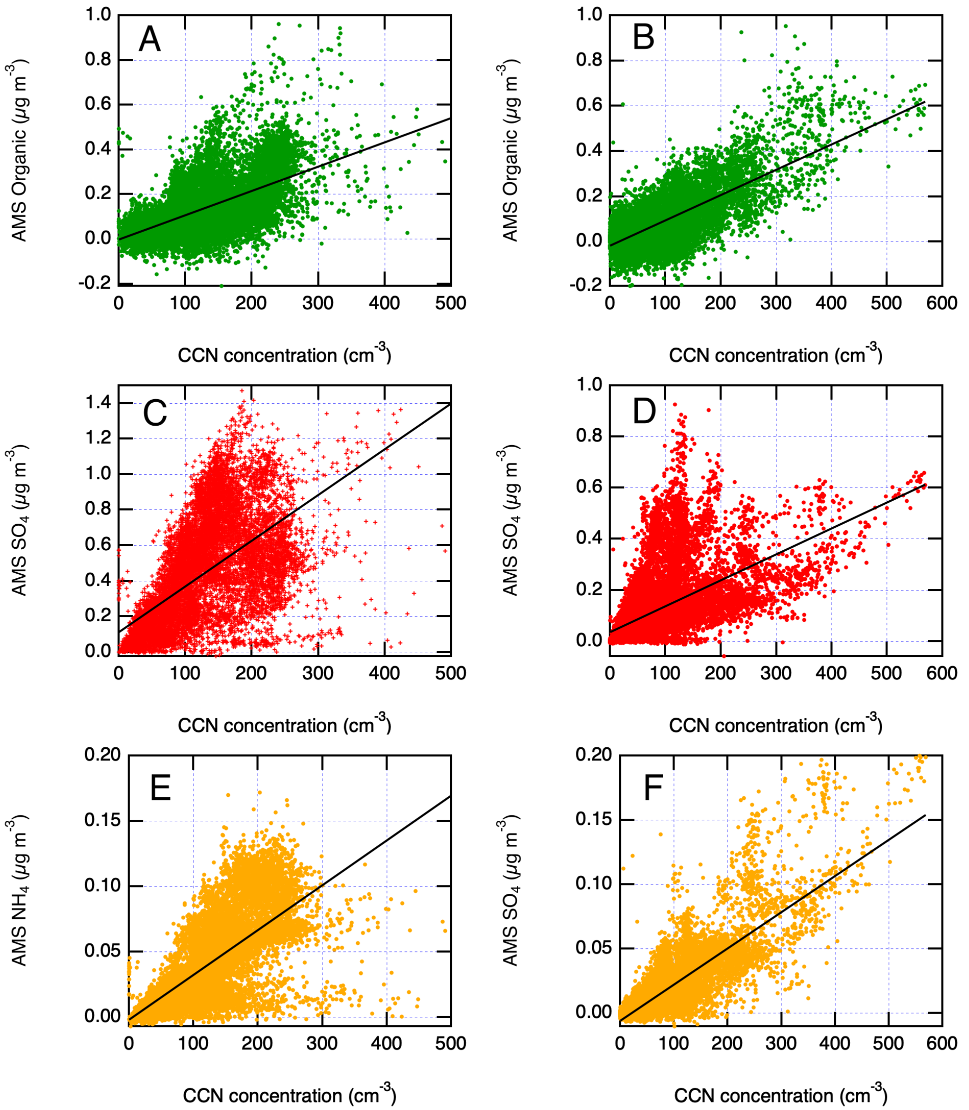

Supplementary Figure S4: Campaign-wide correlations between aerosol chemistry and CCN concentrations at 0.3% supersaturation. (A) AMS organic vs. CCN count, < 1000 m (R^2 = 0.4). (B) AMS organic vs. CCN count, > 1000 m (R^2 = 0.6). (C) AMS SO_4 vs. CCN count, < 1000 m (R^2 = 0.4). (D) AMS SO_4 vs. CCN count, > 1000 m (R^2 = 0.3). (E) AMS NH_4 vs. CCN count, < 1000 m (R^2 = 0.5). (F) AMS NH_4 vs. CCN count, > 1000 m (R^2 = 0.7).

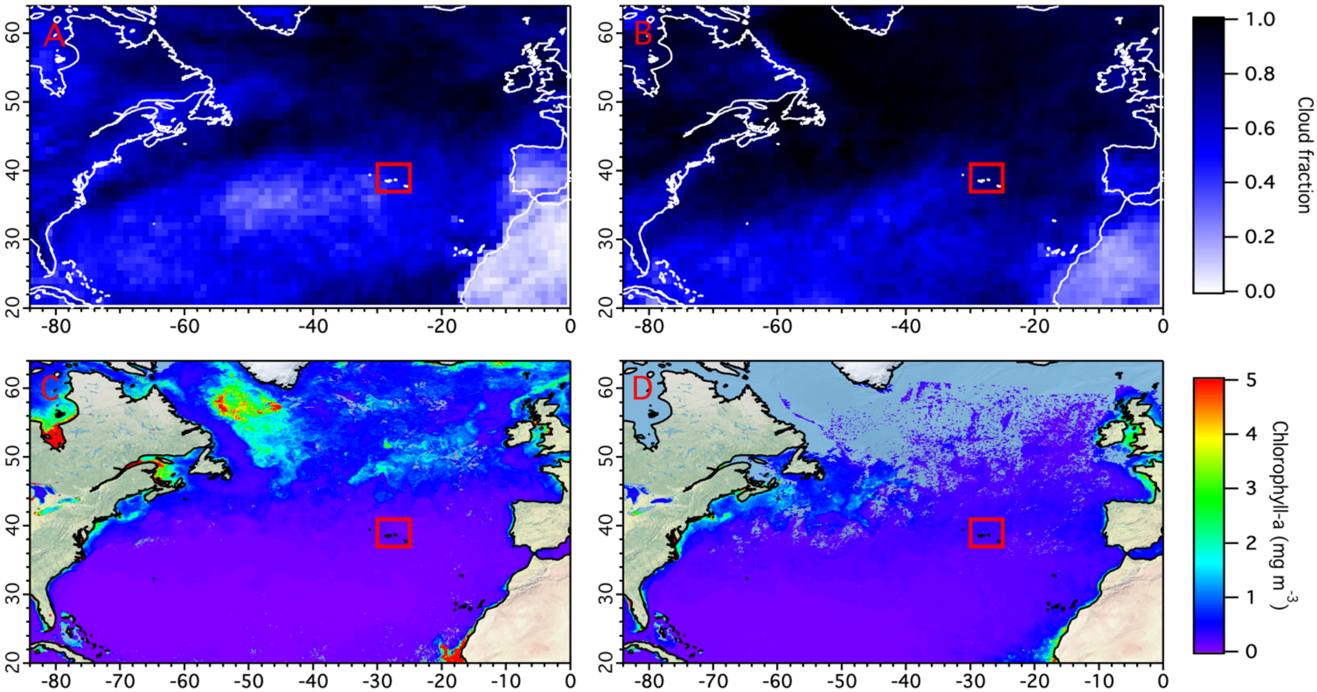

Supplementary Figure S5: Satellite measurements of relevant cloud and biogeochemical parameters during ACE-ENA. (A) MODIS Aqua time-averaged map of cloud fraction from cloud mask (count of lowest 2 clear sky confidence levels, cloudy and probably cloudy divided by the total count). Mean of daily mean, 1º resolution, from 06/21/2017 to 07/20/2017 (IOP 1) (Platnick, 2015). (B) Same as (A) but from 01/19/2018 to 02/19/2018 (IOP 2). (C) MODIS Aqua time-averaged map of chlorophyll-a concentration. Mean of 8-day means, 4 km resolution, 06/18/2017 to 07/28/2017 (IOP 1) (NASA Goddard Space Flight Center, 2018). (D) Same as (C) but from 01/17/2018 to 02/26/2018 (IOP 2). Red box indicates the Azores. The map was created using public domain map data on Natural Earth (naturalearthdata.com) and the GSHHG Database (ngdc.noaa.gov/mgg/shorelines/).

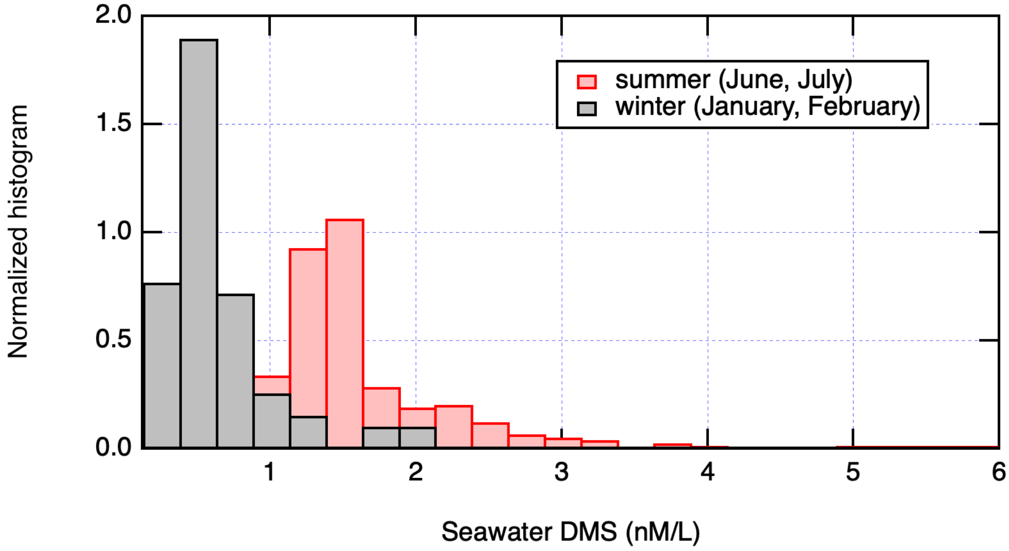

Supplementary Figure S6: The Global Surface Seawater DMS Database (saga.pmel.noaa.gov/dms/) (Kettle et al., 1999) was used to find surface seawater DMS measurements during January and February (n = 78) and June and July (n = 293) in latitudes between 30.7ºN and 48.4ºN and longitudes between 12.6ºW and 38.4ºW (enclosing the Azores).

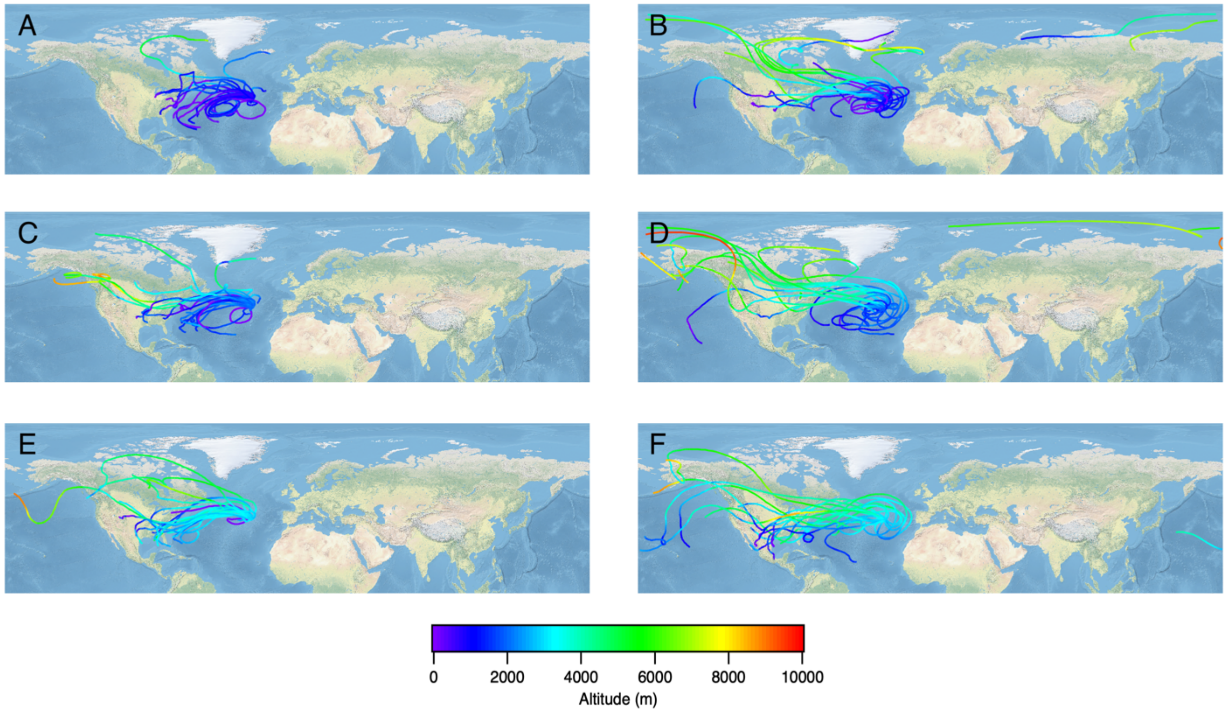

Supplementary Figure S7: HYSPLIT 14-day back-trajectories for each flight. The starting point is the ENA ARM site. (A) 1000 m starting altitude, IOP 1. (B) 1000 m starting altitude, IOP 2. (C) 2000 m starting altitude, IOP 1. (D) 2000 m starting altitude, IOP 2. (E) 3000 m starting altitude, IOP 1. (F) 3000 m starting altitude, IOP 2. The map was created using public domain map data on Natural Earth (naturalearthdata.com) and the GSHHG Database (ngdc.noaa.gov/mgg/shorelines/).

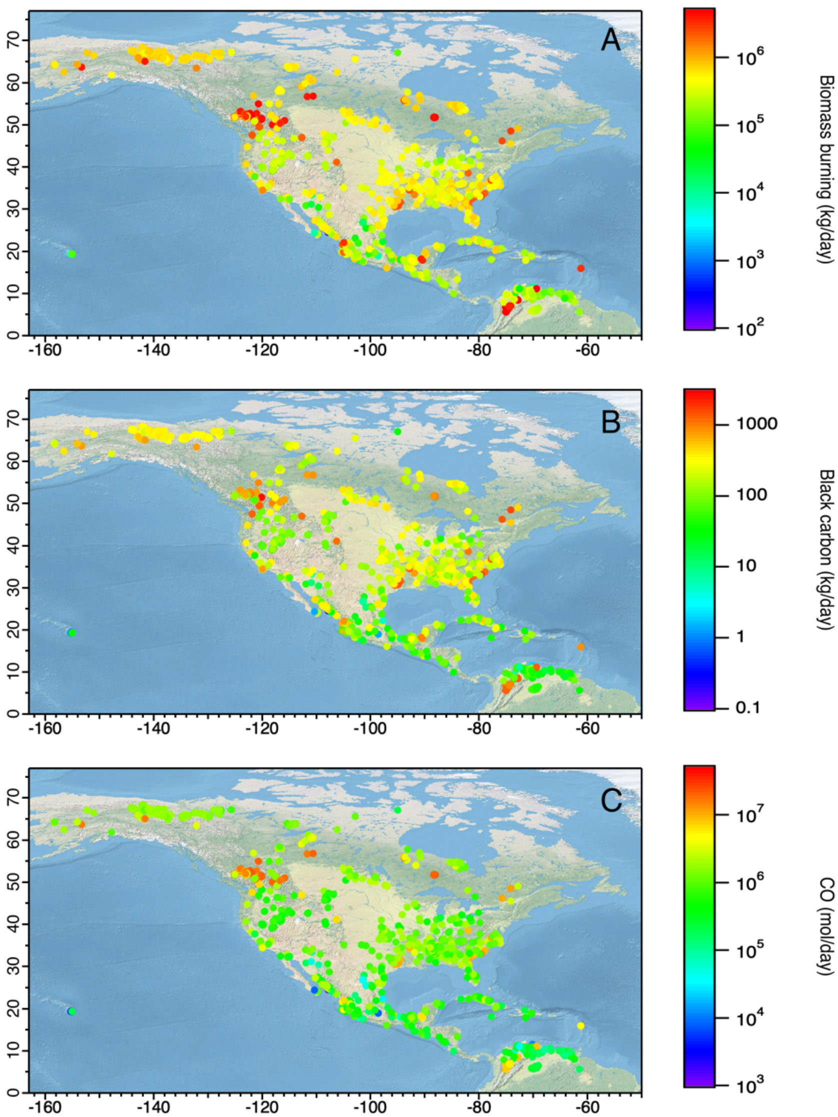

Supplementary Figure S8: Fire emissions during July 12 - 15, 2017 estimated using the Fire Inventory from NCAR (FINN) (Wiedinmyer et al., 2011). (A) Biomass burning emissions. (B) Black carbon emissions. (C) CO emissions. The map was created using public domain map data on Natural Earth (naturalearthdata.com) and the GSHHG Database (ngdc.noaa.gov/mgg/shorelines/).

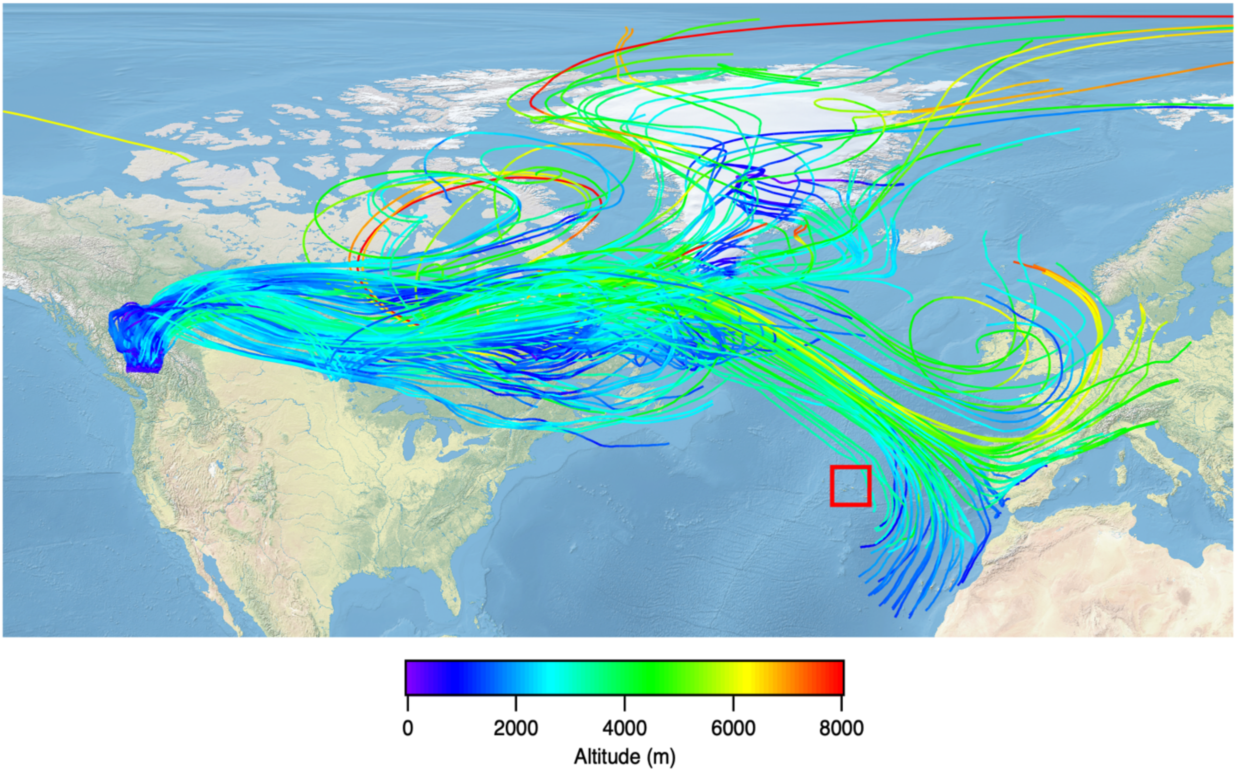

Supplementary Figure S9: HYSPLIT trajectory analysis for the case study of RF #19 (July 19, 2017). A matrix of 121 10-day forward-trajectories was started from an evenly spaced grid bounded by (53.4 N, 125 W), (53.4 N, 121 W), (51 N, 125 W) and (51 N, 121 W) at 500 m altitude. GDAS 0.5 degree meteorology and isentropic vertical motion were used. The red box indicates the location of the Azores. The map was created using public domain map data on Natural Earth (naturalearthdata.com) and the GSHHG Database (ngdc.noaa.gov/mgg/shorelines/).

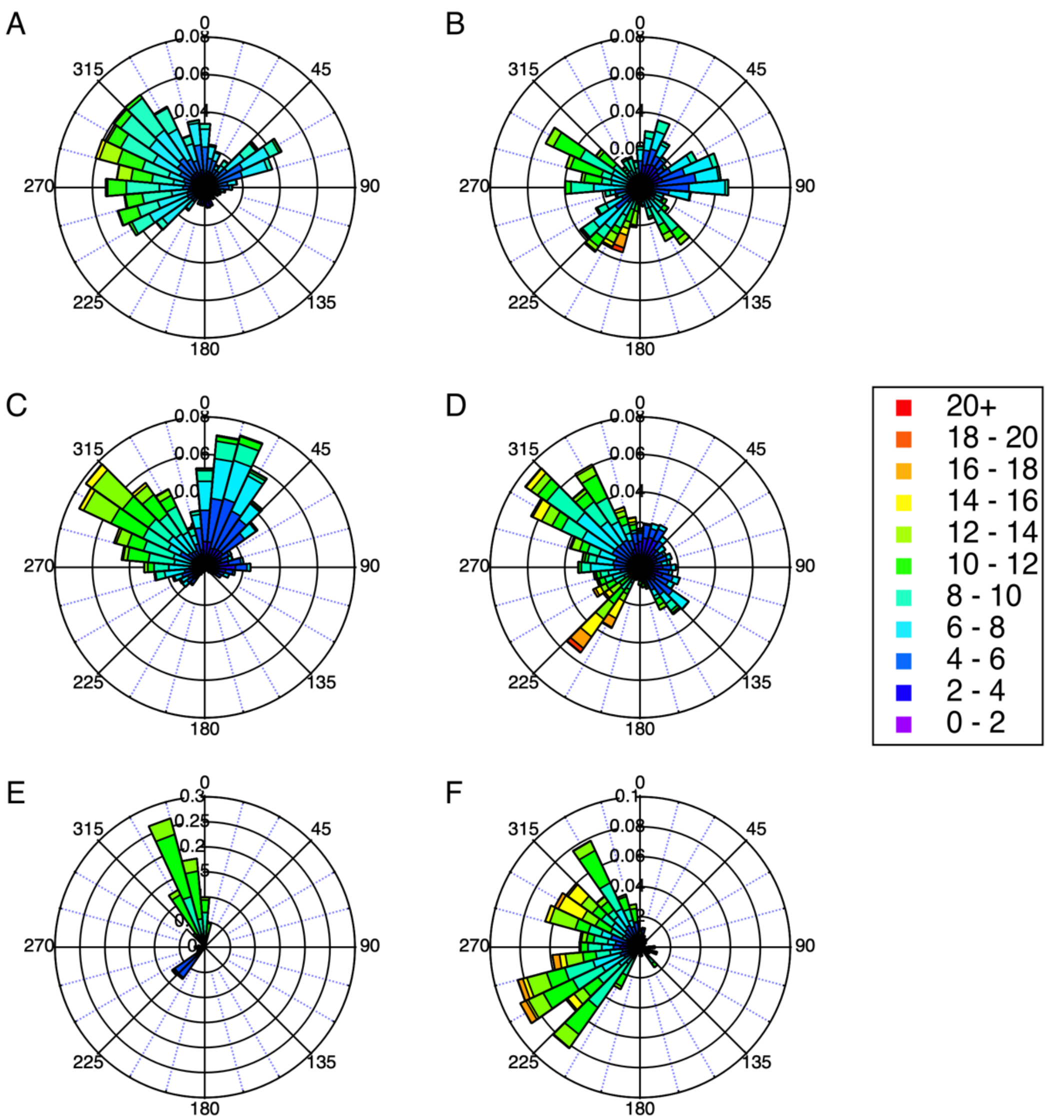

Supplementary Figure S10: Wind roses plotted using data from the G-1 AIMMS-20 probe during all ACE-ENA flights. (A) < 1000 m altitude, IOP 1. (B) < 1000 m altitude, IOP 2. (C) 1000 m - 3000 m altitude, IOP 1. (D) 1000 m - 3000 m altitude, IOP 2. (E) > 3000 m altitude, IOP 1. (F) > 3000 m altitude, IOP 2.

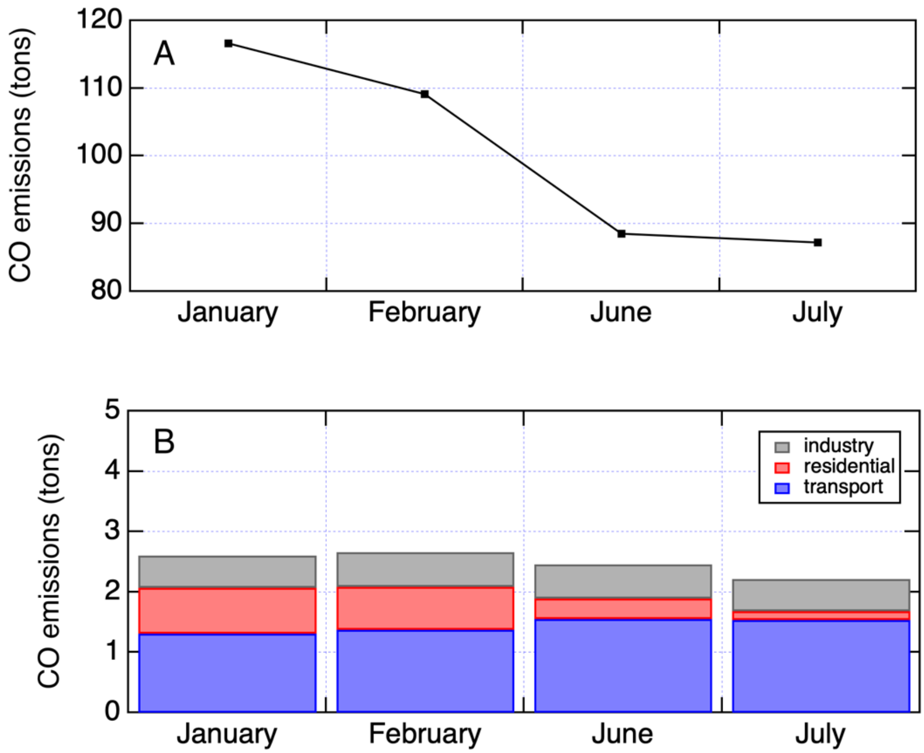

Supplementary Figure S11: EDGAR-HTAP V2 (https://edgar.jrc.ec.europa.eu/htap_v2/) gridded emissions inventory (Janssens-Maenhout et al., 2015) was used to investigate CO emissions from the Azores during the four months of ACE-ENA study. Monthly gridmaps 0.1x0.1 for 2010 were used for this plot. (A) CO emissions from the energy sector. Data from one gridpoint at 38.7ºN, 27.2ºW is available for the Azores. (B) CO emissions from industry, residential and transport sectors. Data from 87 gridpoints are available for the Azores (34ºN - 42ºN, 20ºW - 35ºW), averages by sector are reported in the plot.

References

Ge, X., Zhang, Q., Sun, Y., Ruehl, C. R., and Setyan, A.: Effect of aqueous-phase processing on aerosol chemistry and size distributions in Fresno, California, during wintertime, Environmental Chemistry, 9, 10.1071/en11168, 2012.

Hodshire, A. L., Campuzano-Jost, P., Kodros, J. K., Croft, B., Nault, B. A., Schroder, J. C., Jimenez, J. L., and Pierce, J. R.: The potential role of methanesulfonic acid (MSA) in aerosol formation and growth and the associated radiative forcings, Atmospheric Chemistry and Physics, 19, 3137-3160, 10.5194/acp-19-3137-2019, 2019.

Huang, D. D., Li, Y. J., Lee, B. P., and Chan, C. K.: Analysis of organic sulfur compounds in atmospheric aerosols at the HKUST supersite in Hong Kong using HR-ToF-AMS, Environ Sci Technol, 49, 3672-3679, 10.1021/es5056269, 2015.

Huang, S., Poulain, L., van Pinxteren, D., van Pinxteren, M., Wu, Z., Herrmann, H., and Wiedensohler, A.: Latitudinal and Seasonal Distribution of Particulate MSA over the Atlantic using a Validated Quantification Method with HR-ToF-AMS, Environ Sci Technol, 51, 418-426, 10.1021/acs.est.6b03186, 2017.

Janssens-Maenhout, G., Crippa, M., Guizzardi, D., Dentener, F., Muntean, M., Pouliot, G., Keating, T., Zhang, Q., Kurokawa, J., Wankmüller, R., Denier van der Gon, H., Kuenen, J. J. P., Klimont, Z., Frost, G., Darras, S., Koffi, B., and Li, M.: HTAP_v2.2: a mosaic of regional and global emission grid maps for 2008 and 2010 to study hemispheric transport of air pollution, Atmospheric Chemistry and Physics, 15, 11411-11432, 10.5194/acp-15-11411-2015, 2015.

Kettle, A. J., Andreae, M. O., Amouroux, D., Andreae, T. W., Bates, T. S., Berresheim, H., Bingemer, H., Boniforti, R., Curran, M. A. J., DiTullio, G. R., Helas, G., Jones, G. B., Keller, M. D., Kiene, R. P., Leck, C., Levasseur, M., Malin, G., Maspero, M., Matrai, P., McTaggart, A. R., Mihalopoulos, N., Nguyen, B. C., Novo, A., Putaud, J. P., Rapsomanikis, S., Roberts, G., Schebeske, G., Sharma, S., Simó, R., Staubes, R., Turner, S., and Uher, G.: A global database of sea surface dimethylsulfide (DMS) measurements and a procedure to predict sea surface DMS as a function of latitude, longitude, and month, Global Biogeochemical Cycles, 13, 399-444, 10.1029/1999gb900004, 1999.

Middlebrook, A. M., Bahreini, R., Jimenez, J. L., and Canagaratna, M. R.: Evaluation of Composition-Dependent Collection Efficiencies for the Aerodyne Aerosol Mass Spectrometer using Field Data, Aerosol Science and Technology, 46, 258-271, 10.1080/02786826.2011.620041, 2012.

NASA Goddard Space Flight Center, O. E. L., Ocean Biology Processing Group,: Moderate-resolution Imaging Spectroradiometer (MODIS) Aqua Chlorophyll Data; 2018 Reprocessing, in, NASA OB.DAAC, Greenbelt, MD, USA, 2018.

Ovadnevaite, J., O'Dowd, C., Dall'Osto, M., Ceburnis, D., Worsnop, D. R., and Berresheim, H.: Detecting high contributions of primary organic matter to marine aerosol: A case study, Geophysical Research Letters, 38, n/a-n/a, 10.1029/2010gl046083, 2011.

Phinney, L., Richard Leaitch, W., Lohmann, U., Boudries, H., Worsnop, D. R., Jayne, J. T., Toom-Sauntry, D., Wadleigh, M., Sharma, S., and Shantz, N.: Characterization of the aerosol over the sub-arctic north east Pacific Ocean, Deep Sea Research Part II: Topical Studies in Oceanography, 53, 2410-2433, 10.1016/j.dsr2.2006.05.044, 2006.

Platnick, S.: MODIS Atmosphere L3 Daily Product, in, edited by: System, N. M. A. P., Goddard Space Flight Center, USA, 2015.

Schmale, J., Schneider, J., Nemitz, E., Tang, Y. S., Dragosits, U., Blackall, T. D., Trathan, P. N., Phillips, G. J., Sutton, M., and Braban, C. F.: Sub-Antarctic marine aerosol: dominant contributions from biogenic sources, Atmospheric Chemistry and Physics, 13, 8669-8694, 10.5194/acp-13-8669-2013, 2013.

Wiedinmyer, C., Akagi, S. K., Yokelson, R. J., Emmons, L. K., Al-Saadi, J. A., Orlando, J. J., and Soja, A. J.: The Fire INventory from NCAR (FINN): a high resolution global model to estimate the emissions from open burning, Geoscientific Model Development, 4, 625-641, 10.5194/gmd-4-625-2011, 2011.

Willis, M. D., Burkart, J., Thomas, J. L., Köllner, F., Schneider, J., Bozem, H., Hoor, P. M., Aliabadi, A. A., Schulz, H., Herber, A. B., Leaitch, W. R., and Abbatt, J. P. D.: Growth of nucleation mode particles in the summertime Arctic: a case study, Atmospheric Chemistry and Physics, 16, 7663-7679, 10.5194/acp-16-7663-2016, 2016.

Zorn, S. R., Drewnick, F., Schott, M., Hoffmann, T., and Borrmann, S.: Characterization of the South Atlantic marine boundary layer aerosol using an aerodyne aerosol mass spectrometer, Atmospheric Chemistry and Physics, 8, 4711-4728, 10.5194/acp-8-4711-2008, 2008.